Shape-Adaptive Guidance Signal for Interactive Cortical Sulcal Labeling

Jiwon Son[1] [0009−0005−8897−0945], Ethan H. Willbrand[2] [0000−0003−4625−5642], Benjamin J. Parker[3], Kevin S. Weiner[3] [0000−0002−8734−5049], and Ilwoo Lyu[⋆1] [0000−0001−5868−9603]

[1] Graduate School of Artificial Intelligence, POSTECH, Pohang, South Korea
[2] School of Medicine and Public Health, University of Wisconsin, Madison, WI, USA
[3] Helen Wills Neuroscience Institute, University of California, Berkeley, CA, USA
ilwoolyu@postech.ac.kr

Abstract. We present a spherical CNN-based interactive segmentation framework that leverages a shape-adaptive guidance signal for labeling cortical sulci in the lateral prefrontal cortex (LPFC). Recent neuroscience studies have examined the relationship between sulcal morphology and human cognition, focusing on small and shallow sulci that emerge late in gestation. Due to their variable locations and shapes, these sulci are identified manually by trained raters, which is a labor-intensive process that limits sample sizes in analyses. Although spherical CNN-based automatic sulcal labeling has shown reasonable accuracy for large, consistent sulci, labeling small and variable sulci remains challenging and often requires manual validation and correction. While deep interactive segmentation bridges the gap between manual and automatic labeling, user interactions should be carefully encoded into guidance signals in order to guide the models to accurate refinement. Here, we propose a shape-adaptive guidance signal on the spherical surface, in which the signal is encoded by solving the eikonal equation with a speed function based on mean curvature of the original surface. We compare our method with other guidance signals by training models to label 17 deep and shallow LPFC sulci. Our shape-adaptive signal demonstrates strong initial-click accuracy in small sulci and maintains effective iterative refinement with additional clicks. The code is publicly available at https://github.com/Shape-Lab/ISUS.

Keywords: Interactive segmentation · Spherical CNN · Cortical Sulci · Lateral prefrontal cortex.

1 Introduction

Understanding the link between cortical structure and cognition is a foundational goal in cognitive neuroscience. Sulci, the indentations of the cerebral cortex in gyrencephalic brains, are key morphological features in brain anatomy and development. Recent studies focus on small and shallow sulci in association cortices

⋆ Corresponding Author.

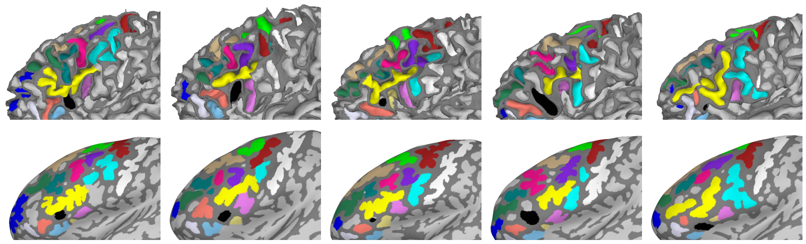

Fig. 1. Anatomical variability in lateral prefrontal cortex. Manually identified sulci are overlaid on the white (*top*) and inflated surfaces (*bottom*). Compared to large and deep sulci, small and shallow sulci show high anatomical variability across individuals. They are occasionally—but not consistently—adjacent to each other in a single component.

like the lateral prefrontal cortex (LPFC) that develop late in gestation [4,25], relating their morphology to higher-order cognition such as reasoning and working memory [23,28,30,26,27]. Accordingly, the growing focus on these small sulci highlights the importance of improving sulcal labeling techniques to accurately capture the finer details and advance our understanding of cortical folds.

Spherical convolutional neural networks (CNNs) have advanced cortical data processing as an invertible spherical mapping is available [5]. Yet, labeling small and shallow sulci remains challenging due to their variability in location, shape, and adjacency, as illustrated in Fig. 1. Furthermore, the limited number of manually labeled data makes it difficult for models to learn individual sulcal variability. Although several spherical CNN-based approaches have shown promise for fully automatic sulcal labeling [8,14,10,11], shallow sulci continue to require expert validation and correction due to their inconsistent morphology. Therefore, cortical sulci are manually identified by trained raters in neuroscience studies. This labor-intensive process bottlenecks the study sizes and underscores the need for reliable labeling tools with minimal user intervention.

Deep interactive segmentation bridges manual and automatic labeling by using sparse human inputs such as clicks or scribbles to guide precise segmentation. Most existing interactive frameworks are mainly focused on 2D images and volumetric data in Euclidean spaces [13,20,16], while their extension to non-Euclidean modalities such as 3D point clouds and surface meshes is relatively underexplored. However, integrating interactive segmentation with spherical CNNs introduces additional challenges. In this setting, the user interactions must be properly encoded into guidance signals on the surface, whose representation has a substantial impact on the labeling performance [16]. A naive approach based solely on spatial proximity overlooks detailed anatomical structure, which may lead to suboptimal refinement in the context of fine-grained sulcal labeling.

In this paper, we propose a novel shape-adaptive guidance signal for interactive cortical sulcal labeling. User interactions are encoded by solving the eikonal equation with a curvature-based isotropic speed function, which propagates signals fast in sulcal regions and slowly in gyri to capture fine-grained

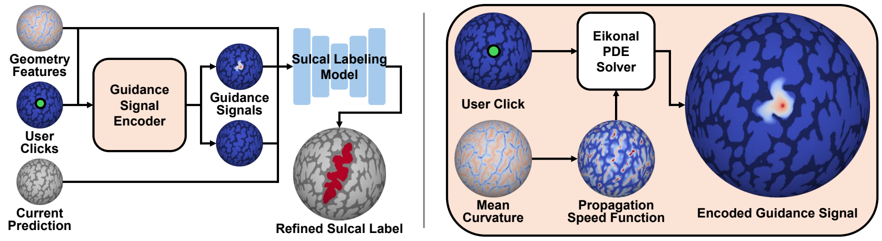

Fig. 2. An overview of the proposed interactive framework (*left*) and guidance signal encoder (*right*). The model uses geometry features, positive or negative clicks encoded as separate channels, and current prediction. The guidance signals are encoded by solving the eikonal equation with a speed function that propagates signals along sulci.

anatomical features. Evaluated on 17 large and small LPFC sulci, the proposed guidance signal achieves higher accuracy with a single click against automatic labeling methods. Compared to other simple encoding schemes, the proposed signal shows higher initial click accuracy in small and variable sulci and enables subsequent performance gains followed by additional clicks.

2 Method

2.1 Problem Statement

Our interactive sulcal labeling model performs binary segmentation of a cortical surface for individual sulci. Since the cortical surface is genus-zero, the features can be mapped onto a unit sphere, simplifying our problem on a spherical domain. For each user click at a spherical location $\mathbf{x} \in \mathbb{S}^2$, the model takes K-dimensional feature vector, including geometric features, the current prediction, and encoded user guidance signals, as shown in Fig. 2. The model output is a binary discriminant function $\mathcal{F} : \mathbb{R}^K \to \mathbb{R}^2$ to infer labels $z \in \{0, 1\}$.

We train a separate model for each sulcus to account for the distinct sulcal morphology, including size, shape, and branching pattern. We optimize $\mathcal{F}$ to iteratively refine a sulcal label with user interactions obtained by the simulated click sampler. At each iteration, a single click is simulated to refine the current prediction, enabling progressive correction of mislabeled regions.

2.2 Iterative User Click Simulation

At each iteration, we simulate a single user click to correct the current prediction. The click can be either a positive click on an under-segmented region or a negative click on an over-segmented region. We adapt the iterative click simulation strategy [15,20] that simulates one click at a time and updates the label each time. First, the manual label is compared with the current prediction to identify the largest mislabeled connected component from either a false-positive or false-negative region. Once the component is identified, geodesic distances from its

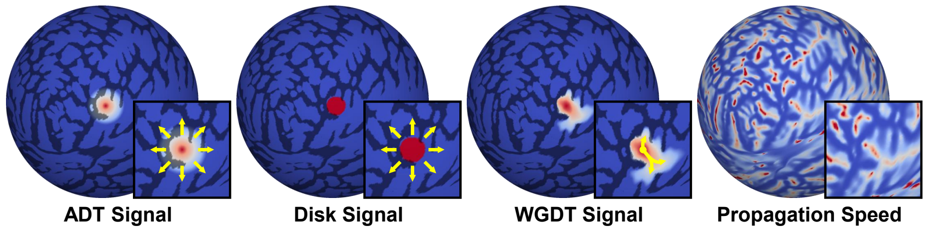

Fig. 3. Guidance signals. Cortical folding patterns are overlaid to each of the signals for better visual inspection. The Angular Disk Transform (ADT) and Disk signals are based on equidistance, while the Weighted Geodesic Distance Transform (WGDT) signal is designed to follow cortical folding patterns.

boundary to interior points are computed. The points with distances below the median value are filtered out to avoid sampling too close to the boundary. The distances of the remaining points are normalized by their maximum distance, and softmax is applied to assign a weight to each point. Finally, weighted random sampling is performed to sample a click. This strategy encourages sampling near the center of the largest mislabeled region, mimicking human refinement.

2.3 Guidance Signal Encoding

For CNN-based interactive segmentation, user interactions are encoded as explicit guidance signals on the spatial domain. The guidance signal provides a localized cue to guide the model in correcting inaccurate predictions. The model refines the label by combining the imaging data, current prediction, and guidance signal. Given the use of spherical CNN in our study, the guidance signals are encoded as spherical signals. To this end, we introduce two approaches: equidistance-based and shape-adaptive signals (see example signals in Fig. 3).

Angular Distance Transform. Encoding a click with distance transform is a popular approach in early studies of CNN-based interactive segmentation [29,12,9]. To extend the Euclidean distance transform from 2D images and 3D volumes to the spherical domain, we encode a click $\mathbf{c} \in \mathbb{S}^2$ using an angular distance transform (ADT). At $\mathbf{x} \in \mathbb{S}^2$, we ensure the signal is bounded in the range $[0, 1]$ and assign higher weights to locations closer to the click point $\mathbf{c}$.

$$\mathrm{ADT}(\mathbf{x}, \mathbf{c}, \sigma) = \begin{cases} 1 - \frac{1}{\sigma} \arccos\left(\mathbf{x} \cdot \mathbf{c}\right) & \text{if } \arccos\left(\mathbf{x} \cdot \mathbf{c}\right) \leq \sigma \\ 0 & \text{otherwise} \end{cases}. \tag{1}$$

Disk. Another commonly used signal is the small-radius binary disk [2,20]. This signal is defined as a binary mask that fills all points within an arc-length (or angle) σ from $\mathbf{c}$. The mask can be defined straightforwardly as

$$\mathrm{Disk}(\mathbf{x}, \mathbf{c}, \sigma) = \begin{cases} 1 & \text{if } \arccos(\mathbf{x} \cdot \mathbf{c}) \leq \sigma \\ 0 & \text{otherwise} \end{cases}. \tag{2}$$

Weighted Geodesic Distance Transform. We hypothesize that adequately covering the target sulcal region in the guidance signal helps the model label the sulci. However, the ADT-based signals rely solely on angular difference between user click and the points on the unit sphere. This approach overlooks the intrinsic morphology of the original cortical surface (see Fig. 3). Consequently, these signals may insufficiently cover the target region or excessively affect neighboring areas, resulting in possible suboptimal refinement. A few studies have proposed geodesic distance transform with pixel or voxel intensity difference in 2D or 3D grid to account for image structure [24,13]. Similarly, to align the guidance signal with the sulcal pattern, the surface geometry must be explicitly considered. To address the issue, we propose a novel guidance signal of weighted geodesic distance transform (WGDT) by performing wavefront propagation on the unit sphere from a click $\mathbf{c}$, with the propagation speed function designed for sulcal labeling. Let $\mathbf{c}$ be a seed point. Following [19], the minimum travel-time (equivalently, distance) $u_{\mathbf{c}}(\mathbf{x})$ from $\mathbf{c}$ to $\mathbf{x} \in \mathbb{S}^2$ meets the propagation equation:

$$\begin{array}{ll} \|\nabla u_{\mathbf{c}}(\mathbf{x})\| F\left(\mathbf{x}, \frac{\nabla u_{\mathbf{c}}(\mathbf{x})}{\|\nabla u_{\mathbf{c}}(\mathbf{x})\|}\right) = 1 & \mathbf{x} \in \mathbb{S}^2 \\ u_{\mathbf{c}}(\mathbf{x}) = 0 & \mathbf{x} \in \mathbf{c} \end{array}, \tag{3}$$

where F is a positive real-valued propagation speed function. We assume F to be an isotropic function, yielding the standard eikonal equation that describes wavefront propagation with a constant speed in all directions at any point. We design F as a spherical function representing the mean curvature derived from the white-matter surface $H : \mathbb{S}^2 \to \mathbb{R}$, so that the signal propagates faster along sulcal region ($H \geq 0$) and slower at gyral region ($H < 0$).

$$F\left(\mathbf{x}, \frac{\nabla u_{\mathbf{c}}(\mathbf{x})}{\|\nabla u_{\mathbf{c}}(\mathbf{x})\|}\right) = e^{kH(\mathbf{x})}, \tag{4}$$

where $k \in \mathbb{R}^+$ is a constant parameter that modulates the influence of H on the propagation speed. Once F is computed, we constrain F within the range $[0.05, 10]$ to mitigate propagation instability. We utilize the fast marching algorithm [18] for solving the above equation on a discrete surface. After solving Eq. 3, the WGDT signal is given by

$$\mathrm{WGDT}(\mathbf{x}, \mathbf{c}, \sigma) = \begin{cases} 1 - \frac{1}{\sigma} u_{\mathbf{c}}(\mathbf{x}) & \text{if } u_{\mathbf{c}}(\mathbf{x}) \leq \sigma \\ 0 & \text{otherwise} \end{cases}, \tag{5}$$

where σ is the maximum travel time of the propagation to localize the feedback. Higher weights are assigned to points closer to $\mathbf{c}$.

2.4 Iteratively Weighted Sulcal Labeling Loss

Following the previous studies on cortical sulcal labeling [14,10], we use cross-entropy loss to minimize the error between the predicted probability p from $\mathcal{F}$ and the manual sulcal label z at each i-th iteration:

$$\mathcal{L}^i_{label} = -\sum_{n\in\{0,1\}} z_n \log(p_n). \tag{6}$$

To encourage iterative refinement, we weight the losses from later iterations more heavily, following the iterative click loss (ICL) approach proposed by [21].

$$\mathcal{L}_{ICL} = \sum_i \beta_i \mathcal{L}^i_{label}, \tag{7}$$

where $\beta_i \in \mathbb{R}^+$ is the weight assigned to the i-th click.

3 Experimental Setup

3.1 Imaging Data

We used a subset of the Human Connectome Project (HCP) [22]. 72 participants were randomly chosen (aged 22-36 years old; 36 males and 36 females). T1-weighted scans were acquired in native space from the HCP dataset [6]. We used geometric features [5]: mean curvature of the white-matter surface (*curv*), average convexity (*sulc*), and mean curvature of the inflated surface (*inflated.H*).

Following the most recent definitions of LPFC sulci [17,23,28,30,26,27], eight large sulci were manually defined: central (cs), superior precentral (sprs), inferior precentral (iprs), inferior frontal (ifs), superior frontal—posterior (sfs-p) and anterior (sfs-a), intermediate frontal—horizontal (imfs-h) and vertical (imfs-v). Nine small, variable sulci were also defined: posterior middle frontal—posterior (pmfs-p), intermediate (pmfs-i), anterior (pmfs-a), diagonal (ds), triangular (ts), ascending (aalf) and horizontal (half) rami of the lateral fissure, pretriangular (prts) and lateral frontomarginal sulcus (lfms). We used the left hemisphere.

3.2 Model Setup

We used SPHARM-Net [7] for our backbone model. We set the entry channels $C = 128$ and the harmonic bandwidth $L = 80$. We used the WGDT signal with $k \in [6, 8, 10]$ and $\sigma = \pi/32$. For comparison, we used ADT and Disk with $\sigma \in [\pi/32, 3\pi/64, \pi/16]$, which are small enough to capture fine-grained sulcal branches. We simulated 3 clicks per subject, accumulating the losses from each of the clicks with $\beta_i \in [1/6, 1/3, 1/2]$. The models were trained using Adam optimizer at an initial learning rate 0.01 with decay by a factor of 0.1 if no improvement is made in two consecutive epochs.

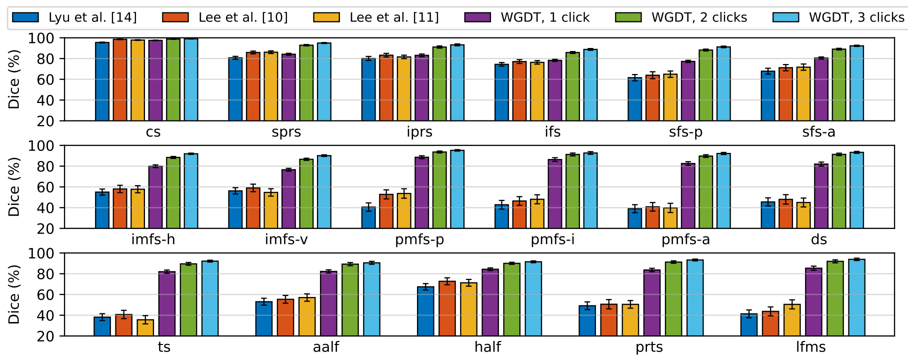

Fig. 4. Region-wise Dice score evaluation of non-interactive baseline against iterative WGDT performance ($k = 8$). The WGDT signal outperforms the baselines with a single click in small and variable sulci.

3.3 Training and Evaluation Criteria

We re-tessellated the spheres by icosahedral subdivision of 40,962 vertices [1]. We performed 5-fold cross validation: 3 partitions for training and 1 each for validation and test. We used Dice score to evaluate the labeling performance. To investigate variable click locations, 10 repeated tests were averaged with different initial clicks generated in a way that each point is located to maximize both the distances from the boundary and the other clicks. To ensure labels were constrained to sulcal regions, outputs with negative *curv* values were discarded. We conducted paired t-tests between WGDT and other encoding schemes. In ROI-wise comparison, multiple-comparison correction among the 17 sulci using false discovery rate (FDR) [3] at $q = 0.05$ was applied. The experiments were performed on Intel Xeon 6526Y and NVIDIA RTX 6000 Ada Generation.

4 Results

We used [14], [10], and [11] for the fully automatic baselines and compared with the proposed method's iterative performance. As shown in Fig. 4, our method outperforms the automatic baselines in small and variable sulci even with a single click, while maintaining comparable Dice scores in large sulci. Existing automatic cortical segmentation networks are prone to individual anatomical variability, occasionally failing to label variable sulci correctly, as observed in Fig. 5. Dice scores improve consistently over iterative clicks, showing that automatic segmentation can be further refined by the proposed framework.

Figure 6 shows the iterative labeling performance comparison among the guidance signals. The proposed signal exhibits the best performance for a single click compared to ADT and Disk, with adjusted $p < 0.05$ for all small and variable sulci. This indicates that a user can label shallow sulci with less effort. These results indicate the importance of the shape-adaptive signal in guiding

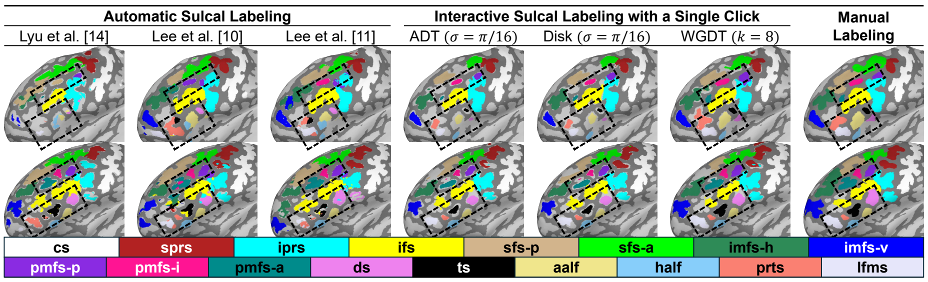

Fig. 5. Visual inspection on two example participants. The WGDT ($k = 8$), ADT and Disk ($\sigma = \pi/16$), whose size sufficiently covers the small sulci, are compared. The WGDT signal well identifies small and variable sulci in LPFC, some of which are not properly located in automatic baselines and are undersegmented in other signals.

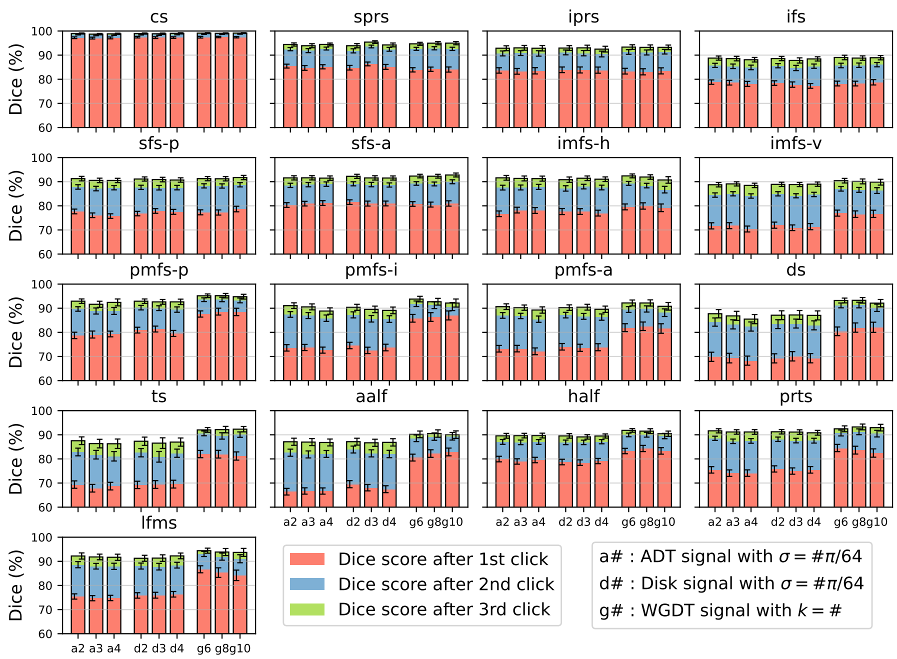

Fig. 6. Region-wise comparison of all guidance signals in iterative refinement. The proposed signal shows significant increase in single-click Dice scores compared to the equidistance-based signals, while retaining the iterative refining performance.

the model to refine sulci. As our backbone model [7] relies on zonal filters, it has a limited representational capacity. The WGDT signal aligns itself with the sulcal patterns, compensating for the filter's low representational capacity and enhancing delineation in small sulci. This is in line with the visualized result in Fig. 5, where the proposed signal identifies the shallow sulci, while the other signals undersegment the region. The speed function designed for fast propagation along sulci enables the clicks to affect a large area when annotating larger sulci, while covering only a small region for the smaller sulci. This guides the model to better infer the user's intended refining area.

5 Conclusion

In this paper, we proposed a shape-adaptive guidance signal for interactive cortical sulcal labeling in LPFC. By incorporating mean curvature of the original cortical surface in the propagation, we aligned the guidance signal with the sulcal patterns. Experimental results demonstrated that the proposed WGDT signal outperformed conventional equidistance-based signals in small sulci. This highlights the importance of geometry-aware guidance in interactive segmentation and offers a practical tool for efficient cortical sulcal labeling.

Acknowledgments. This work was supported in part by NSF CAREER Award 2042251, in part by the National Research Foundation of Korea (NRF) under RS-2024-00333931 and RS-2025-02216257, and in part by the Institute for Information & Communications Technology Planning & Evaluation (IITP) under RS-2019-II191906.

Disclosure of Interests. The authors have no competing interests in the paper.

References

1. Baumgardner, J.R., Frederickson, P.O.: Icosahedral discretization of the two-sphere. SIAM Journal on Numerical Analysis **22**(6), 1107–1115 (1985)
2. Benenson, R., Popov, S., Ferrari, V.: Large-scale interactive object segmentation with human annotators. In: Proceedings of the IEEE/CVF conference on computer vision and pattern recognition. pp. 11700–11709 (2019)
3. Benjamini, Y., Hochberg, Y.: Controlling the false discovery rate: a practical and powerful approach to multiple testing. Journal of the Royal statistical society: series B (Methodological) **57**(1), 289–300 (1995)
4. Chi, J.G., Dooling, E.C., Gilles, F.H.: Gyral development of the human brain. Annals of Neurology: Official Journal of the American Neurological Association and the Child Neurology Society **1**(1), 86–93 (1977)
5. Fischl, B.: Freesurfer. Neuroimage **62**(2), 774–781 (2012)
6. Glasser, M.F., Sotiropoulos, S.N., Wilson, J.A., Coalson, T.S., Fischl, B., Andersson, J.L., Xu, J., Jbabdi, S., Webster, M., Polimeni, J.R., et al.: The minimal preprocessing pipelines for the human connectome project. Neuroimage **80**, 105–124 (2013)
7. Ha, S., Lyu, I.: Spharm-net: Spherical harmonics-based convolution for cortical parcellation. IEEE Transactions on Medical Imaging **41**(10), 2739–2751 (2022)
8. Hao, L., Bao, S., Tang, Y., Gao, R., Parvathaneni, P., Miller, J.A., Voorhies, W., Yao, J., Bunge, S.A., Weiner, K.S., et al.: Automatic labeling of cortical sulci using spherical convolutional neural networks in a developmental cohort. In: 2020 IEEE 17th International Symposium on biomedical imaging (ISBI). pp. 412–415. IEEE (2020)

9. Hu, Y., Soltoggio, A., Lock, R., Carter, S.: A fully convolutional two-stream fusion network for interactive image segmentation. Neural Networks **109**, 31–42 (2019)
10. Lee, S., Lee, S., Willbrand, E.H., Parker, B.J., Bunge, S.A., Weiner, K.S., Lyu, I.: Leveraging input-level feature deformation with guided-attention for sulcal labeling. IEEE Transactions on Medical Imaging **44**(2), 915–926 (2025). https://doi.org/10.1109/TMI.2024.3468727
11. Lee, S., Son, J., Lee, S., Willbrand, E.H., Parker, B.J., Weiner, K.S., Lyu, I.: Extensive spherical region enlargement with isotropic deformation for sulcal labeling. In: 2025 IEEE 22nd International Symposium on Biomedical Imaging (ISBI). pp. 1–5. IEEE (2025)
12. Li, Z., Chen, Q., Koltun, V.: Interactive image segmentation with latent diversity. In: Proceedings of the IEEE conference on computer vision and pattern recognition. pp. 577–585 (2018)
13. Luo, X., Wang, G., Song, T., Zhang, J., Aertsen, M., Deprest, J., Ourselin, S., Vercauteren, T., Zhang, S.: Mideepseg: Minimally interactive segmentation of unseen objects from medical images using deep learning. Medical image analysis **72**, 102102 (2021)
14. Lyu, I., Bao, S., Hao, L., Yao, J., Miller, J.A., Voorhies, W., Taylor, W.D., Bunge, S.A., Weiner, K.S., Landman, B.A.: Labeling lateral prefrontal sulci using spherical data augmentation and context-aware training. NeuroImage **229**, 117758 (2021)
15. Mahadevan, S., Voigtlaender, P., Leibe, B.: Iteratively trained interactive segmentation. In: Proceedings of the British Machine Vision Conference (BMVC). p. 212. BMVA Press, Newcastle, UK (2018), https://bmva-archive.org.uk/bmvc/2018/contents/papers/0652.pdf
16. Marinov, Z., Stiefelhagen, R., Kleesiek, J.: Guiding the guidance: A comparative analysis of user guidance signals for interactive segmentation of volumetric images. In: International Conference on Medical Image Computing and Computer-Assisted Intervention. pp. 637–647. Springer (2023)
17. Petrides, M.: Atlas of the morphology of the human cerebral cortex on the average MNI brain. Academic Press (2018)
18. Sethian, J.A.: A fast marching level set method for monotonically advancing fronts. proceedings of the National Academy of Sciences **93**(4), 1591–1595 (1996)
19. Sethian, J.A., Vladimirsky, A.: Ordered upwind methods for static hamilton–jacobi equations: Theory and algorithms. SIAM Journal on Numerical Analysis **41**(1), 325–363 (2003)
20. Sofiiuk, K., Petrov, I.A., Konushin, A.: Reviving iterative training with mask guidance for interactive segmentation. In: 2022 IEEE International Conference on Image Processing (ICIP). pp. 3141–3145. IEEE (2022)
21. Sun, S., Xian, M., Xu, F., Capriotti, L., Yao, T.: Cfr-icl: Cascade-forward refinement with iterative click loss for interactive image segmentation. Proceedings of the AAAI Conference on Artificial Intelligence **38**(5), 5017–5024 (Mar 2024). https://doi.org/10.1609/aaai.v38i5.28306, https://ojs.aaai.org/index.php/AAAI/article/view/28306
22. Van Essen, D.C., Ugurbil, K., Auerbach, E., Barch, D., Behrens, T.E., Bucholz, R., Chang, A., Chen, L., Corbetta, M., Curtiss, S.W., et al.: The human connectome project: a data acquisition perspective. Neuroimage **62**(4), 2222–2231 (2012)
23. Voorhies, W.I., Miller, J.A., Yao, J.K., Bunge, S.A., Weiner, K.S.: Cognitive insights from tertiary sulci in prefrontal cortex. Nature Communications **12**(1), 5122 (2021)

24. Wang, G., Zuluaga, M.A., Li, W., Pratt, R., Patel, P.A., Aertsen, M., Doel, T., David, A.L., Deprest, J., Ourselin, S., et al.: Deepigeos: a deep interactive geodesic framework for medical image segmentation. IEEE transactions on pattern analysis and machine intelligence **41**(7), 1559–1572 (2018)
25. Welker, W.: Why does cerebral cortex fissure and fold? a review of determinants of gyri and sulci. Cerebral Cortex: comparative structure and evolution of Cerebral Cortex, Part II pp. 3–136 (1990)
26. Willbrand, E.H., Ferrer, E., Bunge, S.A., Weiner, K.S.: Development of human lateral prefrontal sulcal morphology and its relation to reasoning performance. Journal of Neuroscience **43**(14), 2552–2567 (2023)
27. Willbrand, E.H., Jackson, S., Chen, S., Hathaway, C.B., Voorhies, W.I., Bunge, S.A., Weiner, K.S.: Sulcal variability in anterior lateral prefrontal cortex contributes to variability in reasoning performance among young adults. Brain Structure and Function **229**(2), 387–402 (2024)
28. Willbrand, E.H., Voorhies, W.I., Yao, J.K., Weiner, K.S., Bunge, S.A.: Presence or absence of a prefrontal sulcus is linked to reasoning performance during child development. Brain Structure and Function **227**(7), 2543–2551 (2022)
29. Xu, N., Price, B., Cohen, S., Yang, J., Huang, T.S.: Deep interactive object selection. In: Proceedings of the IEEE conference on computer vision and pattern recognition. pp. 373–381 (2016)
30. Yao, J.K., Voorhies, W.I., Miller, J.A., Bunge, S.A., Weiner, K.S.: Sulcal depth in prefrontal cortex: a novel predictor of working memory performance. Cerebral Cortex **33**(5), 1799–1813 (2023)